A Stabilized Finite Element Formulation For High-Speed Inviscid Compressible Flows Using Finite Calculus

Mohammad Kouhi and Eugenio Oñate

December 2, 2013

Abstract

This paper aims at the development of a new stabilization formulation based on the Finite Calculus (FIC) scheme for solving the Euler equations using the Galerkin finite element method (FEM) on unstructured triangular grids. The FIC method is based on expressing the balance of fluxes in a space-time domain of finite size. It is used to prevent the creation of instabilities typically present in numerical solutions due to the high convective terms and sharp gradients. Two stabilization terms, respectively called streamline term and transverse term, are added via the FIC formulation to the original conservative equations in the space-time domain. An explicit fourth order Runge-Kutta scheme is implemented to advance the solution in time. The presented numerical test examples for inviscid flows prove the ability of the proposed stabilization technique for providing appropriate solutions especially near shock waves. Although the derived methodology delivers precise results with a nearly coarse mesh, a mesh refinement technique is coupled to the solution process for obtaining a suitable mesh particularly in the high gradient zones.

Keywords: High-Speed Compressible Flows; Euler Equations; Stabilized Finite Element; Finite Calculus, Explicit Scheme

1 Introduction

The main difficulty regarding the numerical methods in high-speed compressible flows is the occurrence of numerical instabilities which have two main sources, the high value of convective terms in the original partial differential equation and the sharp gradients and shocks in the localized zones of the solution. Much effort has been spent in developing the so called stabilized numerical schemes for all standard numerical methods such as FD, FV and FE. Two main categories of the stabilization methods are artificial diffusion and limiters.

The idea of the artificial diffusion technique, proposed by Von Neumann and Richtmyer in 1950 [1], is to introduce more diffusion in the flow equations by adding viscous terms to the governing partial differential equations explicitly. Within this context, the finite difference method was investigated by Courant et al. in 1952 [2] and Lax in 1954 [3] to solve high-speed compressible flow problems numerically. Courant et al. [2] introduced the upwind family of finite difference methods which was continued by Godunov in 1959 [4] for developing a new finite difference method based on the solution of the so-called Riemann problem. This original approach generated a series of schemes, known as flux difference splitting methods, that lead to different approximate Riemann solvers proposed by Engquist and Osher [5], Roe [6, 7] and Osher [8]. Lax [3] implemented the traditional first order finite difference for discretization of the Euler and Navier-Stokes equations whereas the development of the second order finite difference methods was provided by Lax and Wendroff [9] and Mac-Cormack [10] who implemented an explicit time integration scheme while Lerat and Peyret [11] presented the implicit one. Based on the finite volume scheme and following the idea of artificial diffusion, an important numerical improvement was conducted by Jameson et al. [12] using a series of second and fourth order stabilization methods. The study of finite volume flux vector splitting for the Euler equations was presented by Anderson et al. [13] where several advantages of the MUSCL-type approach over standard flux-differencing scheme were discussed.

Using the Galerkin finite element method, Hughes and his group [14, 15] developed the classical Streamline-Upwind/Petrove-Galerkin (SUPG), initially proposed by Brooks and Hughes [16] for incompressible flows. Based on the idea of the conservation variable formulation, some improvements were made on the original SUPG method [17, 18]. Using the concept of the SUPG method, several stabilization techniques were introduced such as Taylor-Galerkin [19] and Galerkin least squares (GLS) methods [20–22] which coincided with the original SUPG method under some specified conditions. Using of fractional step method [23, 24], Zienkiewicz and co-workers introduced the characteristic-based split (CBS) method [25–28], which benefited from the anisotropic shock capturing term presented by Codina [29]. Another artificial diffusion scheme was developed by Peraire et al. [30], Morgan et al. [31] and Zienkiewicz and Wu [32]. Recently, the so-called variational multiscale (VMS) method, originally introduced by Hughes [33], has been successfully applied to drive stabilized finite element formulation in flow problems [34–36]. Here we also note the work of Scovazzi et al. [37–39] in the derivation of stabilized FEM via variational multiscale techniques for shock capturing in Lagrangian hydrodynamic problems.

Besides artificial diffusion methods, a second family of stabilization methods, based on the so-called limiters, was derived and has been commonly used in finite volume and finite difference schemes. The method is based on preventing the generation of new extrema in the flow solution in such a way that the values of local minima do not decrease, and the values of local maxima do not increase [40–42]. This approach induced to the Flux Corrected Transport (FCT) scheme, developed by Boris and Book [43], and the Total Variation Diminishing (TVD) method introduced by Harten [44]. A fully multidimensional generalization of the FCT algorithm was proposed by Zalesak [45] and carried over to the finite element method by Parrott and Christie [46], Löhner et al. [47] and Luo et al. [48]. Sanders [49] developed the original TVD method from the explicit/implicit fully discrete scheme to a semi-discrete one, whereas Jameson and Lax [50] derived a general TVD characterization and the necessary conditions for multipoint support in explicit, implicit and semi-discrete formulations. Although the FCT scheme has not reached a significant popularity, the TVD method has been widely used in conjunction with finite difference [51–53], finite volume [54] and finite element [55, 56] methods.

In this paper, the Finite Calculus (FIC) formulation for stabilization of the Euler equations is presented in the context of the Galerkin FEM. During the recent years, the FIC procedure has been successfully implemented for the stabilization of advective-diffusive transport and incompressible fluid flow problems by Oñate and co-workers [57–62]. The FIC method is based on expressing the balance of fluxes in the momentum, mass balance and energy conservation equations in a space-time domain of finite size. It is intended to prevent the creation of instabilities usually presented in the numerical solutions due to the high convective terms and sharp gradients. This leads to a modified non-local form of the standard governing equations in mechanics that incorporate additional residual terms that depend on characteristic lengths in space and time. In the context of the compressible flow equations, the FIC approach introduces two stabilization terms, called the streamline term and the transverse term. Generally, the streamline term is responsible for stabilizing the spurious solutions produced from the convective terms while the transverse term smooths the solution in the high gradient zones within the domain. A fourth order Runge-Kutta scheme has been implemented to advance the solution in time.

Along with an appropriate stabilization technique, a suitable computational mesh can enhance the quality and the precision of the numerical results, specially around zones where the gradient of the solution is high. For this reason, the mesh refinement technique developed by Löhner [63] has been implemented in conjunction with the FIC formulation in order to gain a better enrichment level. It is to be mentioned that a suitable level of accuracy can be obtained from the proposed stabilization technique even using a coarse mesh.

In order to investigate the capability of the proposed adaptive FIC-FEM formulation, some numerical test examples related to inviscid flows are presented. The behavior of the stabilization terms in providing appropriate solutions has been studied especially near shock waves and the stagnation point. It is observed that the usual oscillations observed in the Galerkin FEM, especially near high gradient zones, are eliminated by implementing the proposed stabilization terms without introducing an excessive numerical dissipation. Furthermore, by allowing the mesh adaptation scheme, the quality of the results improves significantly.

The structure of the paper is as follows: Section 2 presents the derivation of the stabilized

Galerkin FEM based on the FIC formulation for analysis of compressible inviscid flows. The mesh refinement technique is introduced in Section 3. The numerical results corresponding to subsonic, transonic and supersonic regimes are shown in Section 4. Conclusions and general remarks are summarized in Section 5.

2 The Compressible Euler Equations

2.1 Governing Differential Equations

The Euler equations are a system of nonlinear partial differential equations that describe the behavior of a compressible and inviscid fluid. These equations are deduced from the integral form of the conservation of mass, momentum and energy. For an arbitrary fixed control volume Ω with boundary Γ, they can be expressed as

$$\frac{\partial \rho}{\partial t} + \frac{\partial}{\partial x_j}(\rho v_j) = 0 \tag{1}$$

$$\frac{\partial (\rho v_i)}{\partial t} + \frac{\partial}{\partial x_j}(\rho v_i v_j) + \frac{\partial p}{\partial x_i} = 0 \tag{2}$$

$$\frac{\partial (\rho e)}{\partial t} + \frac{\partial}{\partial x_j}([\rho e + p] v_j) = 0 \quad \text{in } \Omega \tag{3}$$

where ρ is the density, v_j is the fluid velocity in the j^{th} direction, p is the static pressure and e stands for the total internal energy per unit mass. In the above equations $i, j = 1, n_d$ with n_d is the number of space dimensions ($n_d = 2$ for 2D flow problems).

The standard sum convention for terms with repeated indices is adopted in the paper, unless otherwise specified.

2.2 System of Equations

Equations (1), (2) and (3) can be grouped together to form a system of equations. For two dimensional (2D) problems, this system of equations can be expressed as

$$\frac{\partial \mathbf{\Phi}}{\partial t} + \frac{\partial \mathbf{F}_i}{\partial x_i} = \mathbf{0} \quad \text{for} \quad i = 1, 2 \tag{4}$$

where $\mathbf{\Phi}$ is the vector of conservative variables and $\mathbf{F}$ is the vector of inviscid fluxes which have the expressions

$$\mathbf{\Phi} = \begin{bmatrix} \rho \\ U_1 \\ U_2 \\ \rho e \end{bmatrix} \qquad \mathbf{F}_i = \begin{bmatrix} U_i \\ v_i U_1 + p\delta_{i1} \\ v_i U_2 + p\delta_{i2} \\ v_i(p + \rho e) \end{bmatrix} \tag{5}$$

with $U_i = \rho v_i$ and δ_{ij} is the Kronecker delta.

By assuming that the fluid behaves as a perfect gas, the pressure p is obtained from the equation of state given by

$$p = (\gamma - 1)\rho(e - 0.5 v_j v_j) \tag{6}$$

where the ratio of specific heats γ is defined as

$$\gamma = \frac{C_p}{C_v} \tag{7}$$

In the present computations γ is taken to be equal to 1.4 for the air, which is an adequate choice for subsonic, transonic and supersonic flows where the Mach number is not excessively high and chemical reactions can be neglected.

3 A FIC-based Stabilized Formulation

In this section the FIC formulation for stabilization of the Euler equations for compressible flows is presented. The FIC formulation in space is developed for the the momentum and energy conservation equations whereas the representation of the FIC in space-time is used for the mass conservation equation. By combining the three FIC-based conservation equations, the general stabilized formulation of the Euler equations is finally obtained.

3.1 FIC in Space for the Momentum and Energy Equations

We define r_{m_i} and r_e as the residuals of the ith momentum equation and the energy equation, respectively, as

$$r_{m_i} := \frac{\partial(\rho v_i)}{\partial t} + \frac{\partial}{\partial x_j}(\rho v_i v_j) + \frac{\partial p}{\partial x_i} = 0 \tag{8}$$

$$r_e := \frac{\partial(\rho e)}{\partial t} + \frac{\partial}{\partial x_j}(v_j(\rho e + p)) = 0 \tag{9}$$

where $i, j = 1, n_d$.

The FIC formulation in space for stabilizing the momentum and energy equations can be found by re-expressing the momentum and energy conservation equations using higher order Taylor series expansions for expressing the change of the relevant variables over a space domain as

$$r_{m_i} - \frac{1}{2}\mathbf{h}_{m_i}.\boldsymbol{\nabla} r_{m_i} = 0 \tag{10}$$

$$r_e - \frac{1}{2}\mathbf{h}_e.\boldsymbol{\nabla} r_e = 0 \tag{11}$$

where $\mathbf{h}_{m_i}$ and $\mathbf{h}_e$ are characteristic length parameters vectors that will be discussed later.

The derivation of Equations (10) and (11) can be found in [57]. Applications of the FIC approach to incompressible flows and convection-diffusion problems are reported in [58–62].

It can be seen that the modified governing equations via the FIC method introduce naturally an additional term into the standard momentum and energy equations. The definition of the the characteristic length arises from the two main sources of the instabilities in the numerical solution of high-speed compressible flows, namely the high value of the convective terms and the sharp gradients. By considering this fact, the general form of the characteristic length is expressed as

$$\mathbf{h} = \mathbf{h}^v + \mathbf{h}^g \tag{12}$$

where the streamline characteristic length vector $\mathbf{h}^v$ is responsible for smoothing the instabilities due to the high convective terms by adding extra diffusion in the streamline direction, whereas the transverse characteristic length vector $\mathbf{h}^g$ introduces an isotropic (residual-based) diffusion matrix that stabilizes the transverse oscillation in sharp internal layers [58, 62].

Definition of the streamline length vector $\mathbf{h}^v$. The basic idea behind the evaluation of $\mathbf{h}^v$ is extracted from the traditional SUPG scheme for stabilization of the incompressible/compressible flow problems, where the diffusion is added in the direction of the velocity. Hence, the characteristic length vector $\mathbf{h}^v$ for the momentum and energy equations can be expressed as

$$\mathbf{h}^v{}_{m_i} = \beta_{m_i}\ell_{m_i}\frac{\mathbf{v}}{|\mathbf{v}| + v_c} \qquad \mathbf{h}^v{}_e = \beta_e\ell_e\frac{\mathbf{v}}{|\mathbf{v}| + v_c} \tag{13}$$

where β_{m_i} and β_e are constant coefficients that range between zero and one, ℓ_{m_i} and ℓ_e are characteristic element sizes corresponding to the momentum and energy equations. $|\mathbf{v}|$ is the module of the velocity vector and $v_c = \sqrt{\gamma\frac{p}{\rho}}$ is the speed of the sound in the flow.

Definition of the transverse length vector $\mathbf{h}^g$. The transverse stabilization terms are needed in zones where there are some high gradients in the solution. Keeping this in mind, vector $\mathbf{h}^g$ is defined as

$$\mathbf{h}^g_{m_i} = (1 - \beta_{m_i})\ell_{m_i}\frac{\boldsymbol{\nabla} v_i}{|\boldsymbol{\nabla} v_i|}\mathrm{sgn}(r_{m_i}) \qquad \mathbf{h}^g_e = (1 - \beta_e)\ell_e\frac{\boldsymbol{\nabla} T}{|\boldsymbol{\nabla} T|}\mathrm{sgn}(r_e) \tag{14}$$

where sgn(.) is the sign function. Accounting for the sign of the residual in Equation (14) ensures the positiveness of the stabilization parameters (see Equation (35)).

By considering Equation (12), the summation of Equations (13) and (14) gives

$$\mathbf{h}_{m_i} = \beta_{m_i}\ell_{m_i}\frac{\mathbf{v}}{|\mathbf{v}|+v_c} + (1-\beta_{m_i})\ell_{m_i}\frac{\boldsymbol{\nabla} v_i}{|\boldsymbol{\nabla} v_i|}\text{sgn}(r_{m_i}) \tag{15}$$

$$\mathbf{h}_e = \beta_e\ell_e\frac{\mathbf{v}}{|\mathbf{v}|+v_c} + (1-\beta_e)\ell_e\frac{\boldsymbol{\nabla} T}{|\boldsymbol{\nabla} T|}\text{sgn}(r_e) \tag{16}$$

Substituting the characteristic lengths $\mathbf{h}_{m_i}$ and $\mathbf{h}_e$ in Equations (10) and (11), the FIC formulation for the momentum and energy equations is obtained as

$$r_{mi} - \frac{1}{2}(1-\beta_{m_i})\ell_{m_i}\text{sgn}(r_{m_i})\frac{\boldsymbol{\nabla} v_i}{|\boldsymbol{\nabla} v_i|}.\boldsymbol{\nabla} r_{mi} - \frac{1}{2}\beta_{m_i}\ell_{m_i}\frac{\mathbf{v}}{|\mathbf{v}|+v_c}.\boldsymbol{\nabla} r_{m_i} = 0 \tag{17}$$

$$r_e - \frac{1}{2}(1-\beta_e)\ell_e\text{sgn}(r_e)\frac{\boldsymbol{\nabla} T}{|\boldsymbol{\nabla} T|}.\boldsymbol{\nabla} r_e - \frac{1}{2}\beta_e\ell_e\frac{\mathbf{v}}{|\mathbf{v}|+v_c}.\boldsymbol{\nabla} r_e = 0 \tag{18}$$

3.2 FIC in Space-Time for the Mass Conservation Equation

The residual of the mass conservation equation r_d can be expressed as

$$r_d := \frac{\partial \rho}{\partial t} + \frac{\partial(\rho v_j)}{\partial x_j} = 0 \tag{19}$$

with $j = 1, n_d$.

The FIC formulation in space-time is used for deriving the stabilization terms corresponding to the mass balance equation. In the same manner as for obtaining the FIC equations in the space domain, the space-time FIC formulation can be introduced by considering the mass balance equation in a space-time domain. After relatively simple algebra, the FIC formulation for the mass balance equation can be expressed as [57, 62]

$$r_d - \frac{1}{2}\mathbf{h}_d.\boldsymbol{\nabla} r_d + \frac{1}{2}\tau_d\frac{\partial r_d}{\partial t} = 0 \tag{20}$$

where $\mathbf{h}_d$ and τ_d are the characteristic length vector and the time stabilization parameter corresponding to the mass balance equation, respectively, which will be defined later.

It can be seen that the space and time derivatives of the original mass balance equation are involved in the stabilized equation (20). By substituting r_d from Equation (19) in the time-derivative part of Equation (20) and retaining the terms related to the space derivatives, the following expression is obtained

$$r_d - \frac{1}{2}\mathbf{h}_d.\boldsymbol{\nabla} r_d + \frac{1}{2}\tau_d\frac{\partial^2\rho}{\partial t^2} + \frac{1}{2}\tau_d\frac{\partial}{\partial x_j}\frac{\partial(\rho v_j)}{\partial t} = 0 \tag{21}$$

The term $\frac{\partial^2\rho}{\partial t^2}$ in Equation (21) can be obtained explicitly using a simple backward finite difference scheme. However, in our computations we have found that this term does not play an important role in the stabilized formulation and will be neglected here onwards.

Replacing the term $\frac{\partial(\rho v_j)}{\partial t}$ from Equation (8) into Equation (21) gives

$$r_d - \frac{1}{2}\mathbf{h}_d.\boldsymbol{\nabla} r_d - \frac{1}{2}\tau_d\boldsymbol{\nabla}.(\boldsymbol{\nabla}.\mathbf{F}_m) = 0 \tag{22}$$

where $\boldsymbol{\nabla}.\mathbf{F}_m$ is the the divergence of the flux term corresponding to the momentum equation given by

$$\boldsymbol{\nabla}.\mathbf{F}_{m_i} = \frac{\partial(\rho v_i v_j)}{\partial x_j} + \frac{\partial p}{\partial x_i} \tag{23}$$

The expressions of vector $\mathbf{h}_d$ and τ_d for the mass balance equation are defined as

$$\mathbf{h}_d = (1-\beta_d)\ell_d\frac{\boldsymbol{\nabla}\rho}{|\boldsymbol{\nabla}\rho|}\text{sgn}(r_d) \qquad \tau_d = \beta_d\frac{\ell_d}{|\mathbf{v}|+v_c} \tag{24}$$

where β_d is a constant parameter ($0 \leq \beta_d \leq 1$) and ℓ_d is a characteristic element size.

Substituting Equation (24) into (22), the FIC stabilized formulation for the mass equation is obtained as

$$r_d - \frac{1}{2}(1-\beta_d)\ell_d \ \mathrm{sgn}(r_d)\frac{\boldsymbol{\nabla}\rho}{|\boldsymbol{\nabla}\rho|}.\boldsymbol{\nabla} r_d - \frac{1}{2}\beta_d \ell_d \frac{1}{|\mathbf{v}|+v_c}\boldsymbol{\nabla}.(\boldsymbol{\nabla}.\mathbf{F}_m) = 0 \tag{25}$$

3.3 The General FIC-based Formulation

Having introduced the stabilized formulation for the mass, momentum and energy equations, we present the general formulation for the Euler equations. In our work, accurate results have been obtained for the 2D problems solved by considering the assumptions

$$\ell_d = \ell_{m1} = \ell_{m2} = \ell_e = \ell \tag{26}$$

$$\beta_d = \beta_{m1} = \beta_{m2} = \beta_e = \beta \tag{27}$$

where ℓ is a characteristic element size defined as $\ell = (2\Omega^e)^{1/2}$ where Ω^e is the element area for 2D problems. A value of $\beta = 0.5$ is recommended in practice. The effect of other values for β on the quality of the results is studied in the numerical examples of Section 6.

Note that for $\beta = 0$ a SUPG-type stabilization is recovered. On the other hand $\beta = 1$ introduces the isotropic diffusion term only. For values of $0 \leq \beta \leq 1$ the stabilization terms combine the SUPG and the isotropic diffusion contributions in a proportional manner.

By introducing Equations (26) and (27) into Equations (25), (17) and (18), the general FIC-based stabilized formulation can be expressed as

Momentum

$$r_{mi} - \frac{1}{2}(1-\beta)\ell \ \mathrm{sgn}(r_{mi})\frac{\boldsymbol{\nabla} v_i}{|\boldsymbol{\nabla} v_i|}.\boldsymbol{\nabla} r_{mi} - \frac{1}{2}\beta\ell\frac{\mathbf{v}}{|\mathbf{v}|+v_c}.\boldsymbol{\nabla} r_{m_i} = 0 \tag{28}$$

Energy

$$r_e - \frac{1}{2}(1-\beta)\ell \ \mathrm{sgn}(r_e)\frac{\boldsymbol{\nabla} T}{|\boldsymbol{\nabla} T|}.\boldsymbol{\nabla} r_e - \frac{1}{2}\beta\ell\frac{\mathbf{v}}{|\mathbf{v}|+v_c}.\boldsymbol{\nabla} r_e = 0 \tag{29}$$

Mass balance

$$r_d - \frac{1}{2}(1-\beta)\ell \ \mathrm{sgn}(r_d)\frac{\boldsymbol{\nabla}\rho}{|\boldsymbol{\nabla}\rho|}.\boldsymbol{\nabla} r_d - \frac{1}{2}\beta\ell\frac{1}{|\mathbf{v}|+v_c}\boldsymbol{\nabla}.(\boldsymbol{\nabla}.\mathbf{F}_m) = 0 \tag{30}$$

Equations (30), (28) and (29) are the starting point for deriving the discrete (finite element) form of the stabilized Euler equations in space and time. Clearly, for the infinitesimal case the characteristic length $l = 0$ and the standard balance Equations (19), (8) and (9) can be recovered from the general stabilized formulation. It is noticeable that by expressing the stabilization terms as a function of the residuals of the corresponding balance equations the consistency of the proposed FIC method is enforced.

4 Space-Time Discretization

4.1 Galerkin FE

We can introduce a standard finite element discretization of the conservative variables by choosing C^0 continuous linear interpolation over triangular or tetrahedral elements as

$$\boldsymbol{\Phi} \simeq \bar{\boldsymbol{\Phi}} = \sum_{J=1}^{n} \mathbf{N}_J \bar{\boldsymbol{\Phi}}_J \tag{31}$$

where $n = 3$ for triangles, $\bar{\boldsymbol{\Phi}}$ is the vector containing the approximation of the conservative variables $\boldsymbol{\Phi}$, $\mathbf{N}$ is the matrix of the linear interpolating shape functions and $(.)_J$ denotes the J^{th} nodal values of the unknowns.

By applying the standard weighted residual method to Equations (30), (28) and (29) and integrating by parts the stabilization terms, neglecting the boundary terms, the variational form of the discretized equations is found as

$$\int_{\Omega} \mathbf{W}.\bar{\mathbf{r}}d\Omega + \sum_{e}^{n_{el}} \int_{\Omega_e} \frac{1}{2}\mathbf{S}\frac{\partial \mathbf{W}}{\partial x_i}.\frac{\partial \bar{\tilde{\mathbf{\Phi}}}}{\partial x_i}d\Omega + \sum_{e}^{n_{el}} \int_{\Omega_e} \frac{\tau}{2}\mathbf{A}_i\frac{\partial \mathbf{W}}{\partial x_i}.\bar{\mathbf{r}}_{st}d\Omega = 0 \tag{32}$$

where $\mathbf{W}$ is the standard weigthed function vector, n_{el} is the number of the elements and $i = 1, n_d$. In the following, each term of Equation (32) will be defined. The residual vector $\bar{\mathbf{r}}_{st}$ is (for 2D problems)

$$\bar{\mathbf{r}}_{st} = \begin{bmatrix} \boldsymbol{\nabla}.\bar{\mathbf{F}}_m \\ \bar{r}_{m_1} \\ \bar{r}_{m_2} \\ \bar{r}_e \end{bmatrix} \tag{33}$$

where $\bar{r}_{m_1}$, $\bar{r}_{m_2}$ and $\bar{r}_e$ denote the approximate finite element residuals for the mass, momentum and energy equations, respectively, and $\boldsymbol{\nabla}.\bar{\mathbf{F}}_m$ is the divergence of the approximate finite element flux term corresponding to the momentum equation.

Furthermore, $\bar{\tilde{\mathbf{\Phi}}}$ in Equation (32) is the vector of approximated primitive variables, i.e.

$$\bar{\tilde{\mathbf{\Phi}}} = \begin{bmatrix} \bar{\rho} \\ \bar{v}_x \\ \bar{v}_y \\ \bar{T} \end{bmatrix} \tag{34}$$

Finally, $\tau = \frac{\beta\ell}{|\bar{\mathbf{v}}|+\bar{v}_c}$ is the the time stabilization parameter and the stabilization matrices $\mathbf{S}$ and $\mathbf{A}_i$ have the following form

$$\mathbf{S} = (1-\beta)\ell \begin{bmatrix} \frac{|\bar{r}_d|}{|\boldsymbol{\nabla}\bar{\tilde{\Phi}}_1|} & 0 & 0 & 0 \\ 0 & \frac{|\bar{r}_{m_1}|}{|\boldsymbol{\nabla}\bar{\tilde{\Phi}}_2|} & 0 & 0 \\ 0 & 0 & \frac{|\bar{r}_{m_2}|}{|\boldsymbol{\nabla}\bar{\tilde{\Phi}}_3|} & 0 \\ 0 & 0 & 0 & \frac{|\bar{r}_e|}{|\boldsymbol{\nabla}\bar{\tilde{\Phi}}_4|} \end{bmatrix} \tag{35}$$

$$\mathbf{A}_i = \begin{bmatrix} 1 & 0 & 0 & 0 \\ 0 & \bar{v}_i & 0 & 0 \\ 0 & 0 & \bar{v}_i & 0 \\ 0 & 0 & 0 & \bar{v}_i \end{bmatrix} \tag{36}$$

Using the Galerkin approximation, the weighting functions are taken equal to the interpolation ones ($\mathbf{W} = \mathbf{N}$). By applying integration by parts on the first term of Equation (32) we obtain

$$\begin{aligned} \int_{\Omega} \mathbf{N}.\frac{\partial \bar{\tilde{\mathbf{\Phi}}}}{\partial t}d\Omega &= \int_{\Omega} \frac{\partial \mathbf{N}}{\partial x_i}.\bar{\mathbf{F}}_i d\Omega - \int_{\Gamma} \mathbf{N}.\bar{\mathbf{F}}_n d\Gamma \\ &+ \sum_{e}^{n_{el}} \int_{\Omega_e} \frac{\tau}{2}\mathbf{A}_i\frac{\partial \mathbf{N}}{\partial x_i}.\bar{\mathbf{r}}_{st}d\Omega + \sum_{e}^{n_{el}} \int_{\Omega_e} \frac{1}{2}\mathbf{S}\frac{\partial \mathbf{N}}{\partial x_i}.\frac{\partial \bar{\tilde{\mathbf{\Phi}}}}{\partial x_i}d\Omega \end{aligned} \tag{37}$$

with $i = 1, 2$. In Equation (37) $\bar{\mathbf{F}}_i$ is the ith component of approximated inviscid flux vector $\bar{\mathbf{F}}$ (see Equation (5)) and $\bar{\mathbf{F}}_n = \bar{\mathbf{F}}_i n_i$ is the projection of vector $\bar{\mathbf{F}}$ along the normal vector to the boundary $\mathbf{n} = [n_1, n_2]^T$ (for 2D problems). The different types of the boundary conditions are defined in Section 4.3.

In the right-hand-side of Equation (37), the first integral represents the Galerkin term in a weak form, the third integral corresponds to the elemental contribution of the streamline stabilization

term and the last integral is the elemental contribution of the shock capturing stabilization term. This last term has the form of an isotropic diffusion that depends on the residual of each of the equations.

Note that all the terms in matrix $\mathbf{S}$ are positive, which ensures a positive value of the shock capturing diffusion. This is a consequence of accounting for the sign of the corresponding residual in the definition of the characteristic length vectors $\mathbf{h}^g_{m_i}$, $\mathbf{h}^g_e$ and $\mathbf{h}_d$ in Equations (14) and (24).

It is to be mentioned that, although the proposed stabilized formulation is derived for the Euler equations, the extension of this scheme to the Navier-Stokes equations can be carried out with minor modifications.

4.2 The Fourth Order Runge-Kutta Scheme

After discretization of the Euler equation in space and assembling the element contributions from Equation (37), the global system of discretized equations can be written as

$$\mathbf{M}_{IJ}\frac{\partial \bar{\mathbf{\Phi}}^n_J}{\partial t} = \mathbf{RHS}^n_I \tag{38}$$

with $I, J = 1, n_{node}$ where n_{node} is the total number of nodes in the mesh and $(.)^n$ means the value computed at time step n. In the above equation, $\mathbf{M}_{IJ}$ is the consistent finite element mass matrix

$$\mathbf{M}_{IJ} = \int_\Omega \mathbf{N}_I.\mathbf{N}_J d\Omega \tag{39}$$

Also, $\mathbf{RHS}^n_I$ is the contribution of the Ith global node from the right hand side of Equation (37) in time step n which has the form

$$\begin{aligned}\mathbf{RHS}^n_I = &\left\{\int_\Omega \frac{\partial \mathbf{N}_I}{\partial x_i}.\bar{\mathbf{F}}_i d\Omega - \int_\Gamma \mathbf{N}_I.\bar{\mathbf{F}}_n d\Gamma\right\}^n \\ &+ \left\{\sum_e^{n_{el}} \int_{\Omega_e} \frac{\boldsymbol{\nu}}{2}\frac{\partial \mathbf{N}_I}{\partial x_i}.\frac{\partial \bar{\bar{\mathbf{\Phi}}}}{\partial x_i} d\Omega + \sum_e^{n_{el}} \int_{\Omega_e} \frac{\tau}{2}\mathbf{A}_i \frac{\partial \mathbf{N}_I}{\partial x_i}.\bar{\mathbf{r}}_{st} d\Omega\right\}^n\end{aligned} \tag{40}$$

To avoid solving a linear system of equations at each time step, in our work we have replaced the consistent mass matrix $\mathbf{M}$ by its lumped expression $\mathbf{M}_L$. Furthermore, as the focus of this paper is on stationary problems, an explicit multi-stage Runge-Kutta algorithm is implemented in order to obtain a converged steady state solution,

Assuming that the nodal values $\bar{\mathbf{\Phi}}^n_J$ and $\mathbf{RHS}^n_I$ are known at time t_n, the advance of the solution over the time step t_n to t_{n+1} is as follows

$$\begin{aligned}&\bar{\mathbf{\Phi}}^{(0)}_J = \bar{\mathbf{\Phi}}^n_J \\ &\vdots \\ &\bar{\mathbf{\Phi}}^{(k)}_J = \bar{\mathbf{\Phi}}^n_J + \alpha_k \Delta t [\mathbf{M}_L]^{-1}\mathbf{RHS}^{(k-1)}_I \qquad k = 1, ..., K \\ &\vdots \\ &\bar{\mathbf{\Phi}}^{n+1}_J = \bar{\mathbf{\Phi}}^{(K)}_J\end{aligned} \tag{41}$$

with K being the number of stages of the scheme. Each particular scheme is characterized by a choice of K and the constant coefficients α_k. The appropriate choose of these coefficients improves the stability of the time integration and provides accurate numerical solutions. Good results have been obtained with

$$K = 4 \implies \alpha_1 = 1/4; \alpha_2 = 1/3; \alpha_3 = 1/2; \alpha_4 = 1 \tag{42}$$

The scheme presented here is explicit and therefore only conditionally stable. The stability limit for an element is calculated as [64]

$$\Delta t_e = \mathcal{C}\frac{h}{|\bar{\mathbf{v}}| + \bar{v}_c} \tag{43}$$

where $\mathcal{C}$ denotes the allowable Courant number and $h = \ell$ is the characteristic element size. Except $\mathcal{C}$ which is global, the remaining variables in the above equation are calculated at the element level. If a time accurate solution is sought, the global time step equals to the minimum allowable one for all the elements in the mesh. In order to enhance the performance of the presented time integration scheme, local time stepping and residual smoothing technique are coupled to the solver. More details about these schemes can be found in [65].

4.3 Boundary Conditions

The discretized equation system of Equation (37) assumes a computational domain Ω surrounded by a boundary Γ with unit normal $\mathbf{n}$. So far, the algorithm only describes the contributions of each element across the integral Ω but does not yet states how to incorporate the boundary conditions at the boundary Γ.

In our work, two types of boundaries have been considered: the slip boundary Γ_W through which mass flux is not possible and the far field (inflow/outflow) boundary Γ_∞ through which mass flux is possible. The boundary condition must be applied in a compatible form with the equations to be solved.

Slip Boundary
The normal component of the velocity must vanish on it. This condition can be enforced by considering the normal component of the velocity equal to zero after each stage, k, of the time integration scheme as

$$\mathbf{v}^{(k)}.\mathbf{n} = 0 \quad \text{on} \quad \Gamma_W \tag{44}$$

Far Field Boundary
Depending on the flow regime, the components of the solution which enter the domain are to be enforced and the ones leaving the domain have to be set free. By using Roe approximation for Riemann solvers, the appropriate boundary flux for node I located at the far field boundary is computed as

$$\bar{\mathbf{F}}_n^I = \frac{1}{2}\{\bar{\mathbf{F}}_n(\bar{\mathbf{\Phi}}^I) + \bar{\mathbf{F}}_n(\bar{\mathbf{\Phi}}^\infty) - |\bar{\mathbf{A}}_n(\bar{\mathbf{\Phi}}^I, \bar{\mathbf{\Phi}}^\infty)|(\bar{\mathbf{\Phi}}^I - \bar{\mathbf{\Phi}}^\infty)\} \tag{45}$$

where superscript ∞ represents the freestream value and $\bar{\mathbf{A}}_n(\bar{\mathbf{\Phi}}^I, \bar{\mathbf{\Phi}}^\infty)$ is the Roe matrix computed in the direction normal to the boundary. More details about the derivation of the Roe matrix can be found in [64, 66].

5 Mesh Refinement

The error indicator introduced by Löhner [63] is implemented in this paper. For each variable of interest U, the general form of the error indicator is

$$error(U) = \frac{h^2|second\ derivative\ of\ U|}{h|first\ derivative\ of\ U| + c_n|mean\ value\ of\ U|} \tag{46}$$

where h is the element size and c_n is a constant depending on the discretization technique.

This equation yields bounded and dimensionless values for the error indicator. The variable U is one of the flow variables such as the density, the Mach number, the velocity modulus, etc. In our work, the density has been chosen. The implementation of this error indicator in different engineering applications can be found in [67–69]. The multidimensional form of this error indicator for node I can be expressed as

$$E^I(U) = \sqrt{\frac{\sum_{k,l}(\int_\Omega N^I_{,k}N^J_{,l}\,d\Omega.U^J)^2}{\sum_{k,l}(\int_\Omega |N^I_{,k}|[|N^J_{,l}U^J| + c_n|N^J_{,l}||U^J|]\,d\Omega)^2}} \tag{47}$$

where $(.)_{,k}$ and $(.)_{,l}$ denote the first-order derivative with respect to k^{th} and l^{th} coordinate directions, respectively. N^J and U^J denote the shape function and the flow variable, respectively, corresponding to node J.

The well known h-refinement strategy [63, 67, 68] has been implemented in conjunction with the above error indicator. This strategy is based on the classic subdivision of an element into other four ones (for 2D problems) by dividing each edge of element into two. Indeed, mesh coarsening is another possibility which can be performed by removing elements.

An unstructured grid discretization using 3-noded elements with linear shape functions are considered here. Given the minimum/maximum element size, the constant coefficient c_n and the desired maximum error E_{max} and minimum error E_{min}, several remeshing levels are performed every predefined time steps of the solution process in order to guarantee a fine mesh at the end of the analysis.

The first step in the h-refinement strategy is to identify the element required refinement or coarsening by comparing the actual error obtained from Equation (47) with the predefined E_{max} and E_{min} values. Also, the size of identified elements must be in the range of the desired maximum and minimum element size. In the second step of the h-refinement strategy, the new mesh is created by subdividing or removing the elements corresponding to the refinement or coarsening, respectively. Finally, the values of the unknown flow variables in the new time step using a new mesh are interpolated from the last known values in the previous using a linear interpolation scheme.

6 Test Examples

The performance of the FIC-based stabilization methodology, has been assessed by numerical examples of compressible inviscid flow in subsonic, transonic and supersonic regimes for steady-state problems. All the tests are performed with triangular meshes and an explicit Runge-Kutta time integration scheme where the relative L_2 norm of the density residual is taken as a criterion to check convergence. It is to be mentioned that the computations start by using the upstream values as the initial solution and they are stopped after a reduction of four order of magnitude in the relative L_2 norm of the density residual. If the analytical solution exists, the obtained numerical results are compared with exact solutions, whereas for the rest of cases the comparison is carried out with published results.

All computations are performed using an unstructured mesh which is enhanced by the h-refinement technique, presented in Section 5. It is to be mentioned that the refinement is not implemented in the subsonic example as no shock wave happens in the solution. At the beginning stage of the refinement, the solution starts using an unstructured mesh. Having reached the stationary solution, consecutive refinement levels are carried out every 200 time-steps. Once the final adaptive mesh is obtained, the solution stops when the stationary solution is reached. We note that the initial mesh must be fine enough to be able to capture the main characteristics of the flow in order to detect the regions where mesh refinement is needed.

A value of $\beta = 0.5$ has been used. The sensitivity of the numerical solution to β is studied in Example 6.1.

6.1 Example I: Reflected shock

A popular example for supersonic regime is the reflected shock problem involving an oblique shock at the angle of 29° and its reflection from the boundary. The main feature of this example is that it can be solved analytically.

The problem consists in an uniform flow with Mach 2.0 at the angle of 10° in a rectangle domain of height 4.1 and length 1.1 which involves three flow regions, plotted in Figure 1 schematically, as

Region 1	Region 2	Region 3
$\rho = 1.0$	$\rho = 1.7$	$\rho = 2.6872$
$M = 2.9$	$M = 2.3781$	$M = 1.9423$
$v_1 = 2.9$	$v_1 = 2.6193$	$v_1 = 2.4015$
$v_2 = 0.0$	$v_2 = -0.5063$	$v_2 = 0.0$
$v_c = 1.0$	$v_c = 1.1218$	$v_c = 1.2363$
$p = 0.7143$	$p = 1.5282$	$p = 2.9340$

On the left and upper side of the domain the flow variables of density, velocity and temperature have fixed values corresponding to Region 1 and Region 2, respectively, whereas the lower wall is considered as a no slip boundary where the normal component of the velocity is prescribed as zero. The flow variables on the right side of the domain have been left free.

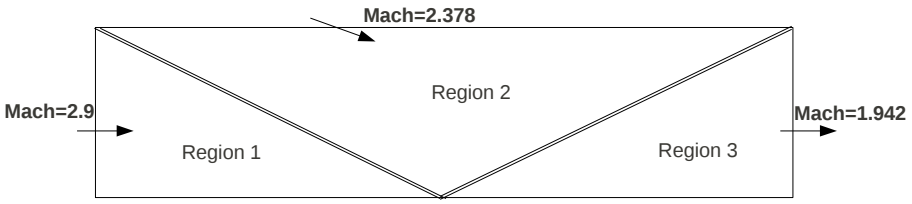

Figure 1: Reflected shock example. Problem definition.

The initial unstructured mesh, shown in Figure 2a, has 1376 nodes and 2580 3-noded triangular elements. The final adaptive mesh of 3352 nodes and 6456 elements is obtained after five steps of refinement as shown in Figure 2b. The form of this mesh clearly demonstrates that the refinement has been carried out along the flow discontinuities.

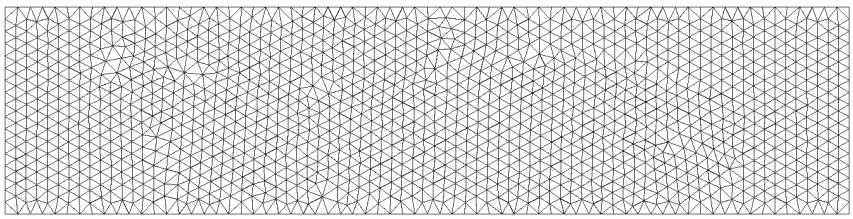

(a)

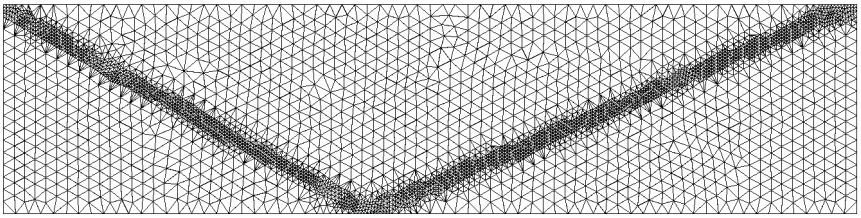

(b)

Figure 2: Reflected shock. (a) Initial mesh and (b) adaptive mesh after 5 refinement levels.

Figures 3 and 4 display numerical results corresponding to the initial and final mesh, respectively, which indicate the smoothness of the solution in all the domain, especially near the shocks. It can be seen that although the FIC method is capable to predicting good results by using a coarse discretization, mesh refinement enhances the resolution of the shocks. An angle of approximately 29° is obtained for the shock by using coarse and fine discretizations which means that the shock locations are captured accurately by the FIC stabilized formulation. We note that the shocks are captured within four or five elements for both discretizations.

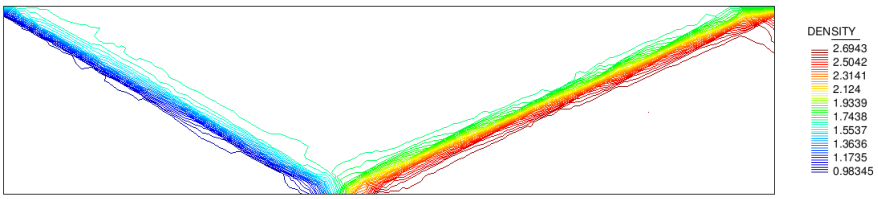

(a)

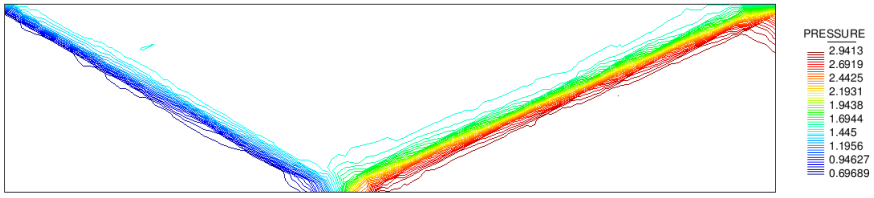

(b)

Figure 3: Reflected shock. The results using initial mesh (a) density contours and (b) pressure contours.

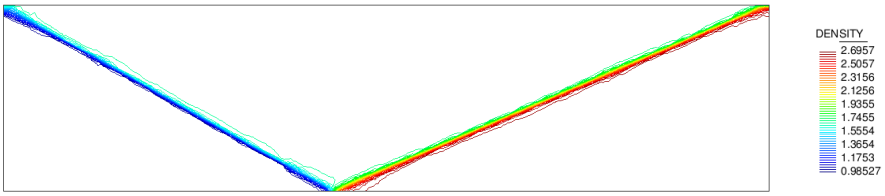

(a)

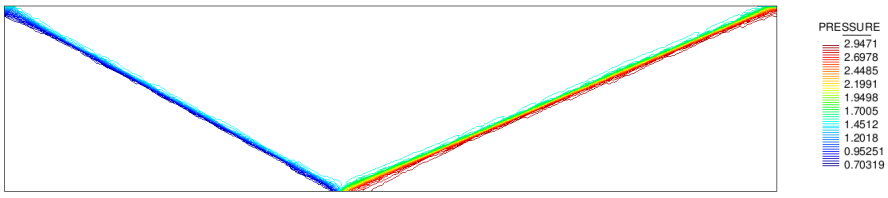

(b)

Figure 4: Reflected shock. The results using adaptive mesh (a) density contours and (b) pressure contours.

The comparison of the density profiles at $y = 0.25$ corresponding to the exact solution and the numerical solution obtained using the initial and the adaptive meshes is depicted in Figure 5. Good agreement with the exact solution is obtained.

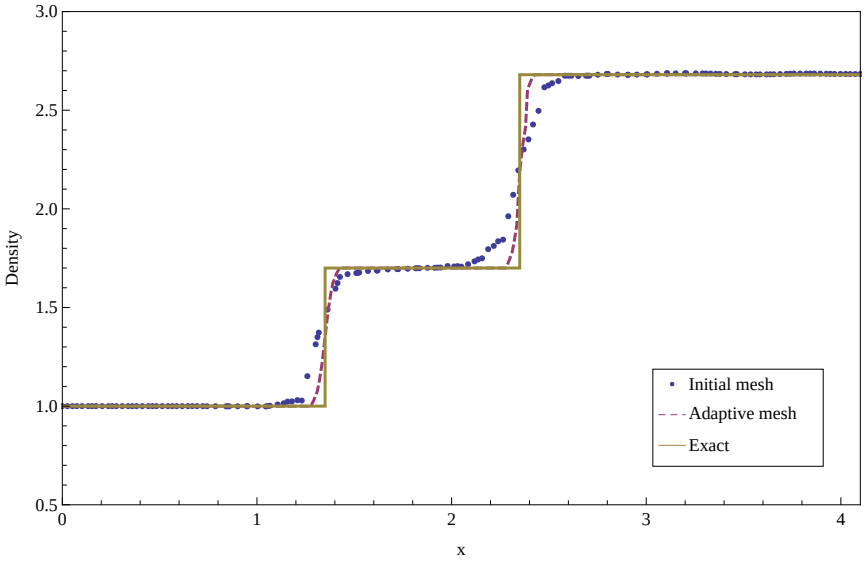

Figure 5: Reflected shock example. Comparison of the density profiles at $y = 0.25$.

The convergence history for this test case is plotted in Figure 6. Remeshing starts after reaching four order reduction in L_2 norm of the density residual followed by consecutive refinement levels every 200 time steps. By using a final adapted mesh after five refinement levels, the computations are continued until a suitable convergence in time is obtained. It is to be mentioned that the peaks of the convergence graph denote each refinement level carried out during the solution process.

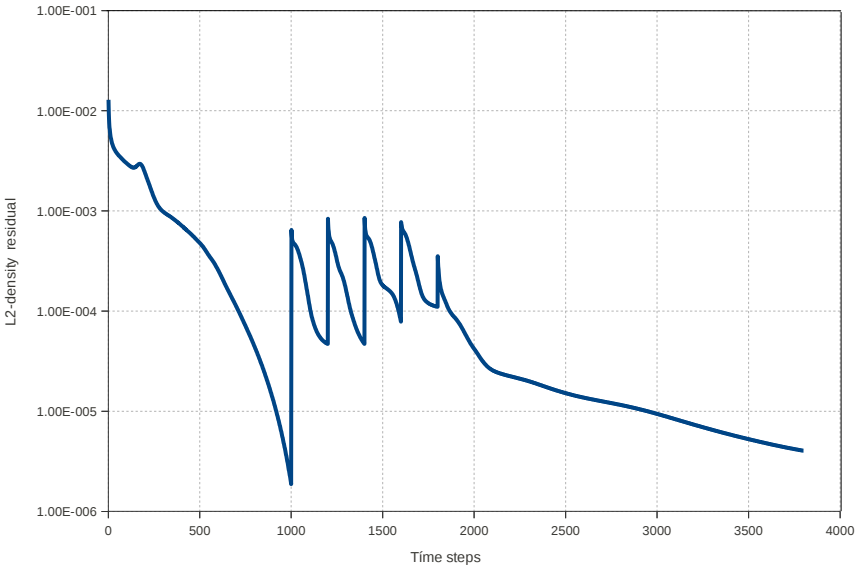

Figure 6: Reflected shock example. Convergence history using five refinement levels.

The capability of the present method for different values of the β coefficient affecting the stabilization terms has been tested. The numerical results corresponding to $\beta = 0.25$ and $\beta = 0.75$ are displayed in Figures 7 and 8, respectively, containing the final adapted meshed, density contours using the uniform and the adapted meshes and the comparison of the density profiles at $y = 0.25$. We have found that the choice of $\beta = 0.25$ yields a more diffusive solution while a sharper shock is obtained by assuming $\beta = 0.75$. Although the shock positions are almost captured by both uniform and adapted meshes, some oscillations are seen in the solution near the shocks. These results justify the choice of $\beta = 0.5$ for practical purposes.

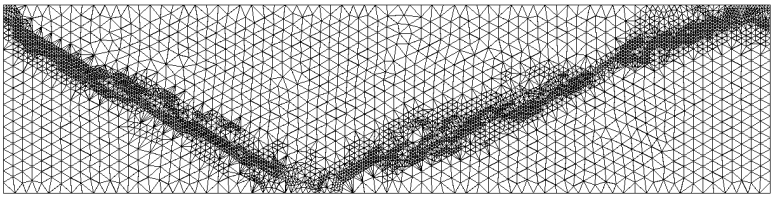

(a)

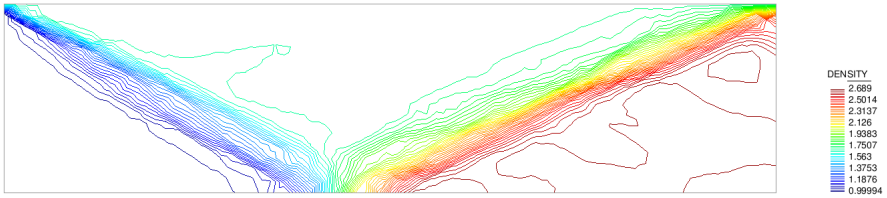

(b)

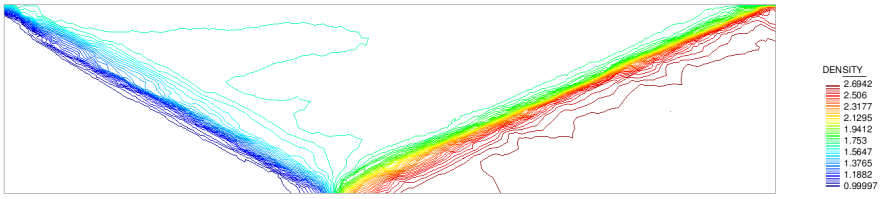

(c)

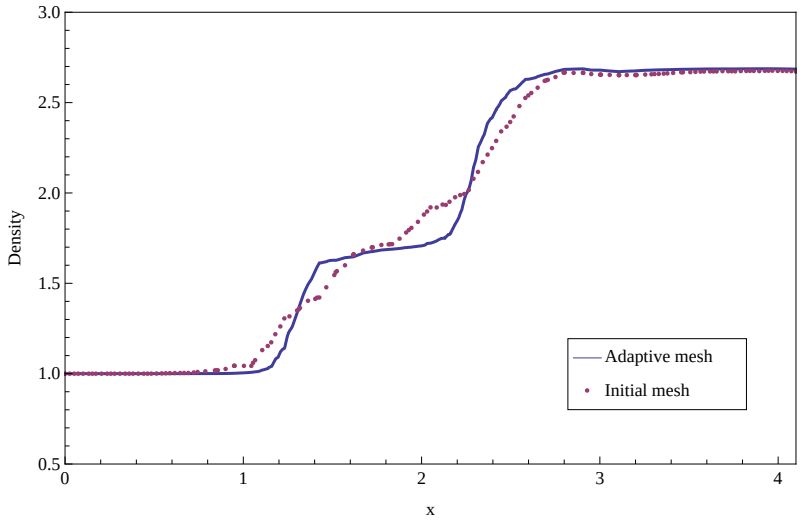

(d)

Figure 7: Reflected shock. Results obtained using $\beta = 0.25$. (a) Adaptive mesh after 5 refinement levels. (b) Density contours using uniform mesh. (c) Density contours using the adaptive mesh. (d) Comparison of the density profiles at $y = 0.25$.

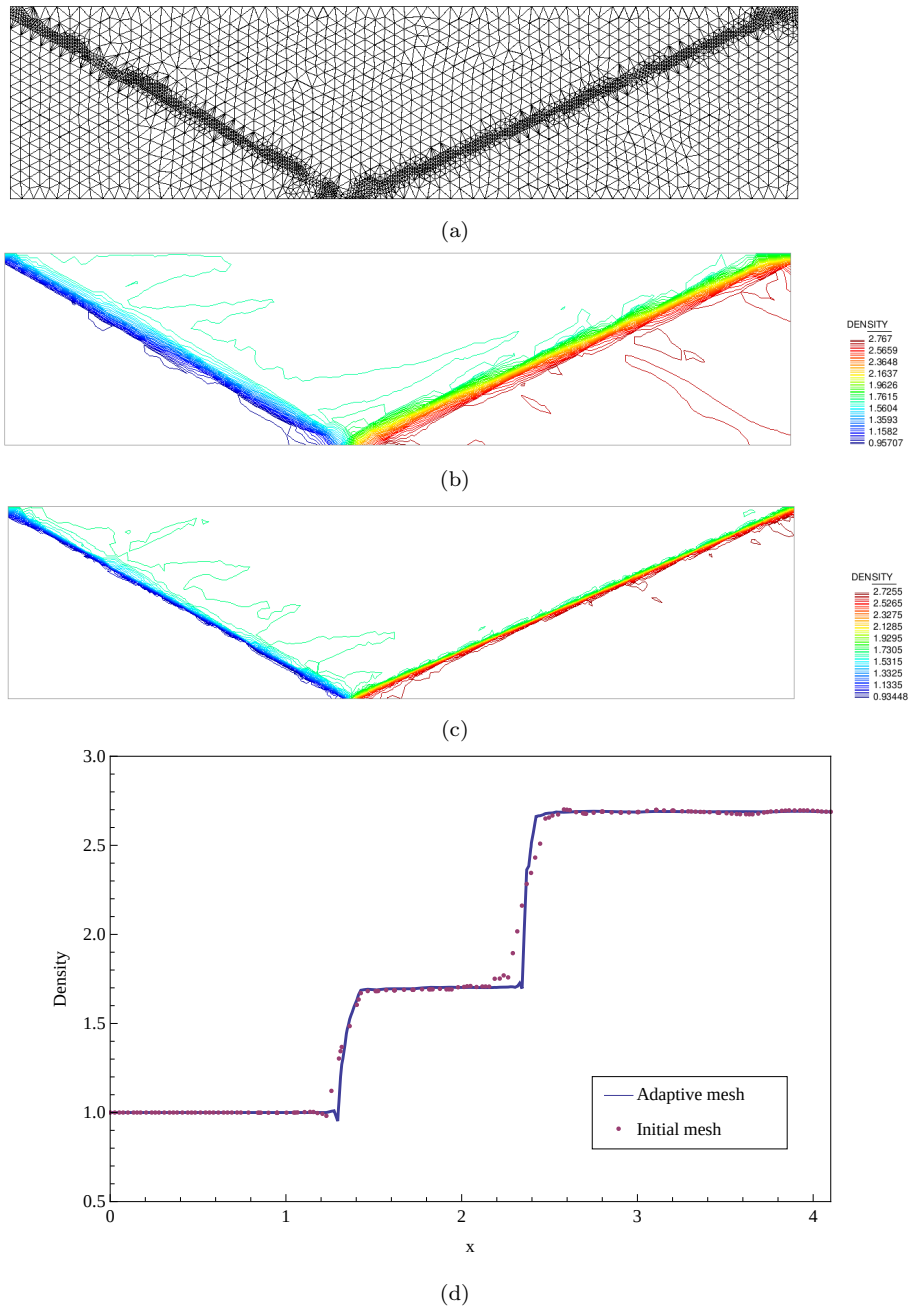

Figure 8: Reflected shock. Results obtained using $\beta = 0.75$. (a) Adaptive mesh after 5 refinement levels. (b) Density contours using uniform mesh. (c) Density contours using the adaptive mesh. (d) Comparison of the density profiles at $y = 0.25$.

6.2 Example II: Subsonic inviscid flow around a NACA0012 airfoil

This example, taken from [27], illustrates the quality of the flow solution for an inviscid subsonic compressible flow past a NACA0012 airfoil at $M_\infty = 0.5$ and $\alpha = 0.0°$ where a circular computational domain with the radius of 8 chords is considered. In order to demonstrate the effect of grid resolution on the behaviour of the proposed scheme, the domain around the airfoil was discretized by setting different values for the number of elements along the airfoil boundary. The airfoil close-up of the coarse mesh, intermediate mesh and fine mesh are shown in Figure 9 while the mesh details are presented in Table 1.

Since the flow does not involve any shock waves, mesh refinement is not employed in this

example. The slip boundary condition is applied on the surface of the airfoil, whereas the far field boundary condition is considered on the outer boundary.

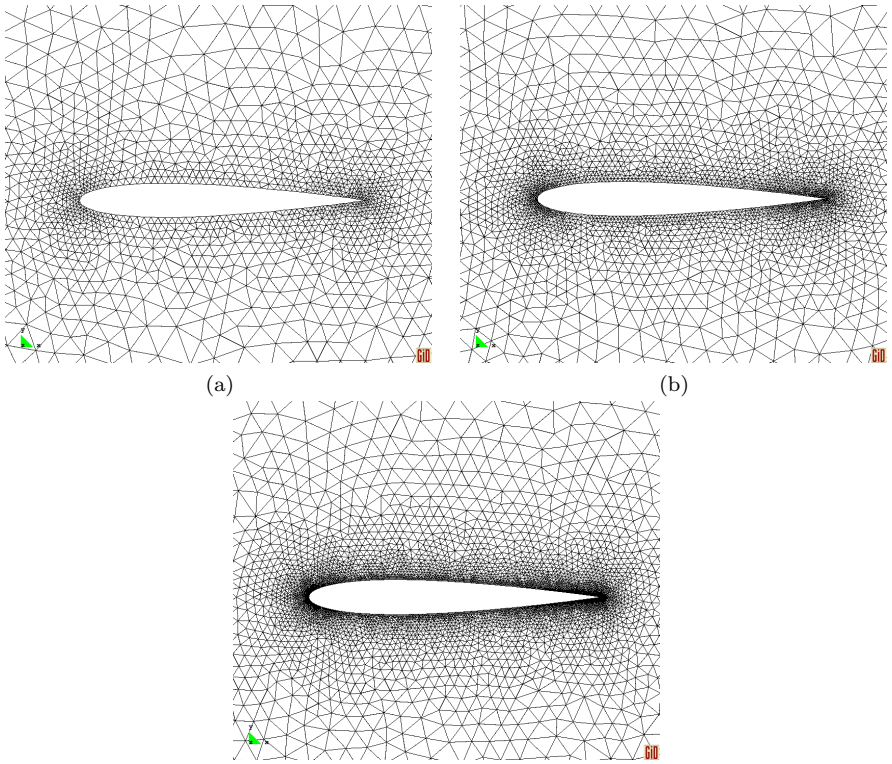

Figure 9: Subsonic inviscid flow around a NACA0012 airfoil. Airfoil close-up of (a) coarse mesh, (b) intermediate mesh and (c) fine mesh.

Table 1: Subsonic inviscid flow around a NACA0012 airfoil. Number of elements along the airfoil, number of nodes and number of elements corresponding to different meshes.

	Coarse Mesh	Intermediate Mesh	Fine Mesh
Airfoil Elements	124	256	472
Nodes	2748	3992	6178
Elements	5496	7984	12356

In Figure 10 the density contours corresponding to the coarse mesh, intermediate mesh and fine mesh are presented demonstrating that no oscillations are observed even for the coarse mesh. A test for accuracy is the value of the density at the stagnation point for which the analytical solution is known, as

$$\rho_0 = \rho_\infty (1 + \frac{\gamma - 1}{2} M_\infty^2)^{\frac{1}{\gamma - 1}} \tag{48}$$

where $\rho_\infty = 1$ and $\gamma = 1.4$ for this example. Inserting $M_\infty = 0.5$, we obtain $\rho = 1.1297$ as the analytical value. The resulted density values at the stagnation point using different meshes along with the corresponding relative errors respect to the analytical value are presented in Table 2. The accuracy of the numerical solution is remarkable. Besides, it can be understood that the accuracy will improve as a finer mesh is implemented.

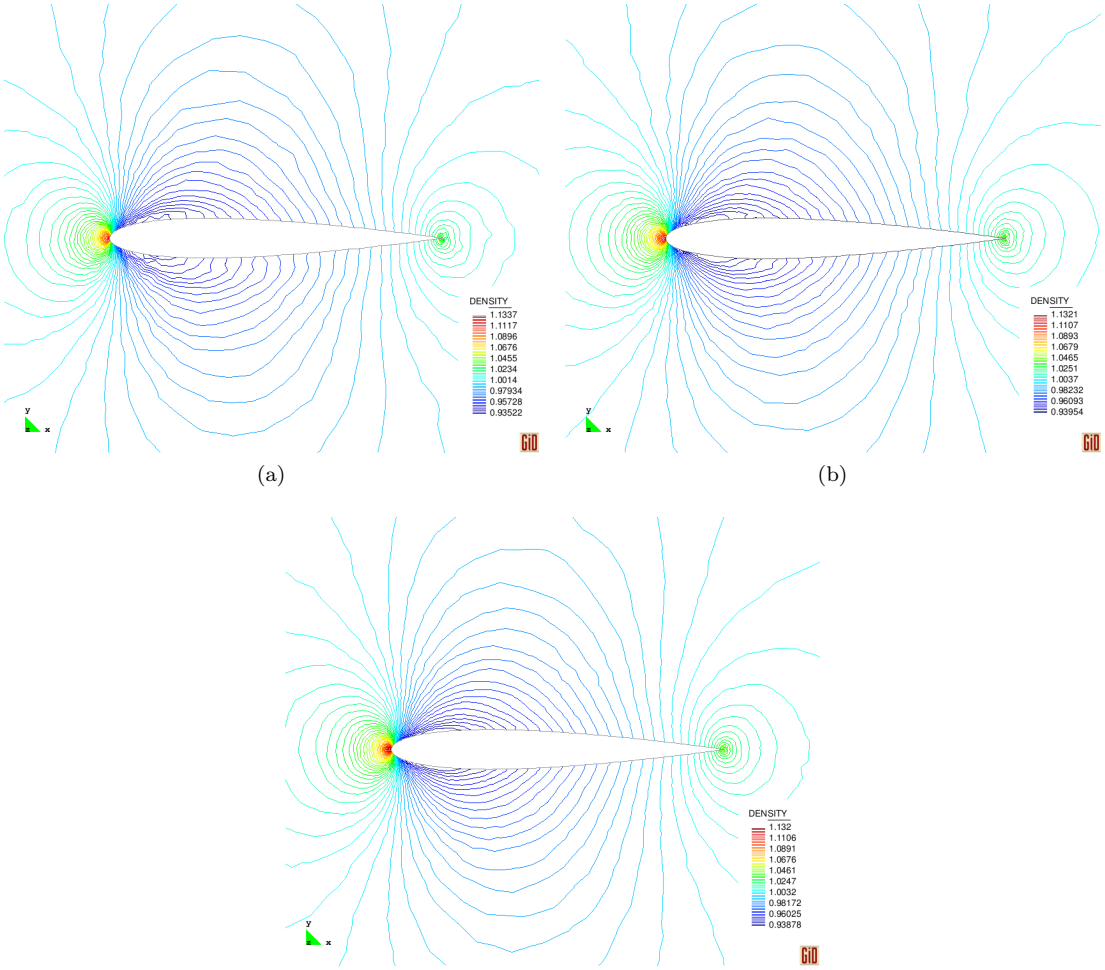

Figure 10: Subsonic inviscid flow around a NACA0012 airfoil example. Density contours around. (a) Coarse mesh. (b) Intermediate mesh. (c) Fine mesh.

Table 2: Subsonic inviscid flow around a NACA0012 airfoil. Density values at the stagnation point obtained from different meshes.

	Coarse Mesh	Intermediate Mesh	Fine Mesh
Density Value	1.1347 (0.45%)	1.1321 (0.21%)	1.1320 (0.20%)

The convergence history of the density at the stagnation point corresponding to different meshes is presented in Figure 11a. Although the FIC formulation using the coarse mesh presents some spurious oscillations, this inappropriate behaviour disappear by implementing the intermediate and fine meshes. The corresponding values along the stagnation streamline are given in Figure 11b showing that smooth solutions are obtained in this zone using different meshes.

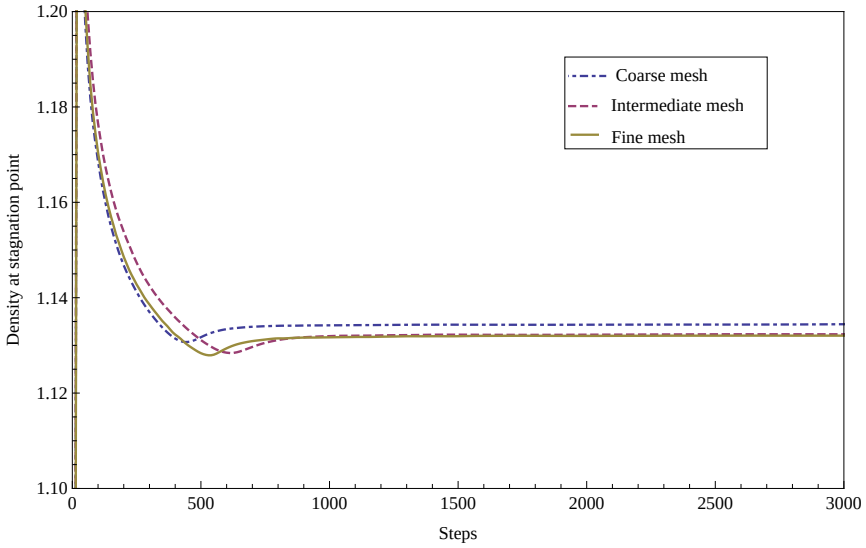

(a)

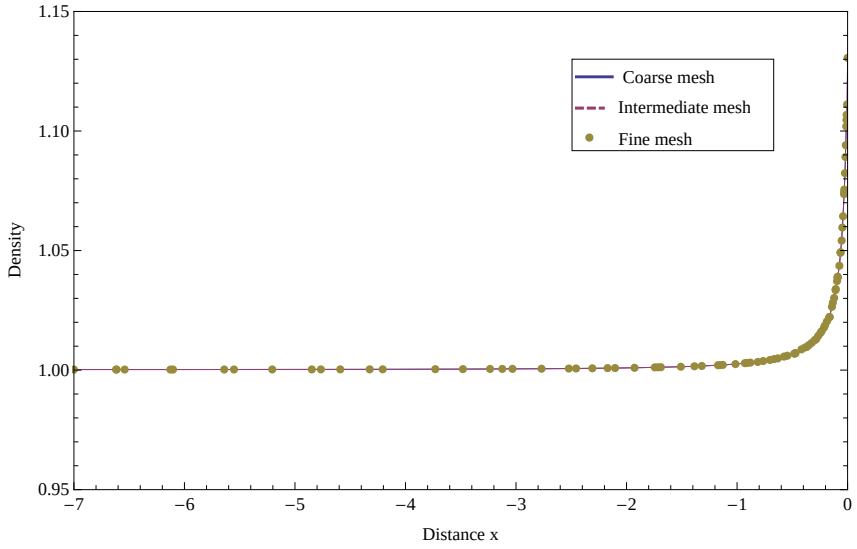

(b)

Figure 11: Subsonic inviscid flow around a NACA0012 airfoil example. (a) Convergence of the density at the stagnation point using different meshes. (b) Density value along the stagnation streamline using different meshes.

6.3 Example III: Transonic inviscid flow around a NACA0012 airfoil

This example demonstrates the ability of the FIC-FEM formulation for the analysis of the transonic compressible flow around a NACA0012 airfoil at $M_\infty = 0.8$ and $\alpha = 1.25°$. This example is taken from the reports of the AGARD Working Group 07 [70]. The initial mesh for this example is the same as the intermediate mesh shown in Figure 9b. The slip boundary condition is assigned on the surface of the airfoil, whereas the far field boundary condition is applied on the outer boundary. The adapted mesh after five steps of refinement, containing 8010 nodes and 15768 elements, is shown in Figure 12 where the concentration of the elements in the vicinity of the high gradient zones is clearly seen.

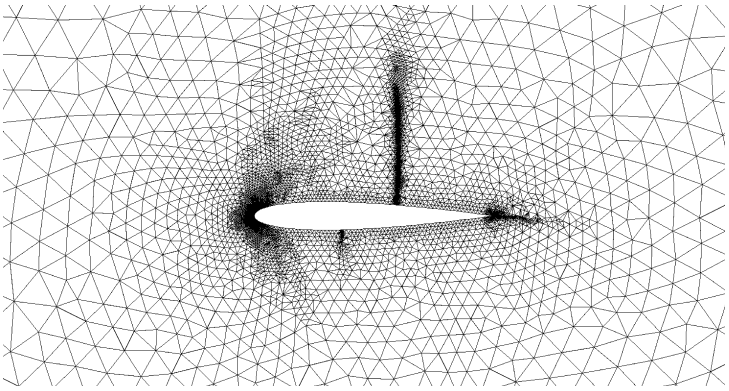

Figure 12: Transonic inviscid flow around a NACA0012 airfoil. Final adapted mesh.

The solution variables corresponding to the initial mesh and the adaptive mesh are presented in Figures 13 and 14 from which the effect of mesh refinement in improving the quality of the results can be observed. It can be found that, using both initial and adaptive discretizations, the stronger shock at the upper side of the airfoil is captured with minor oscillations, as well as the weaker one at the lower side.

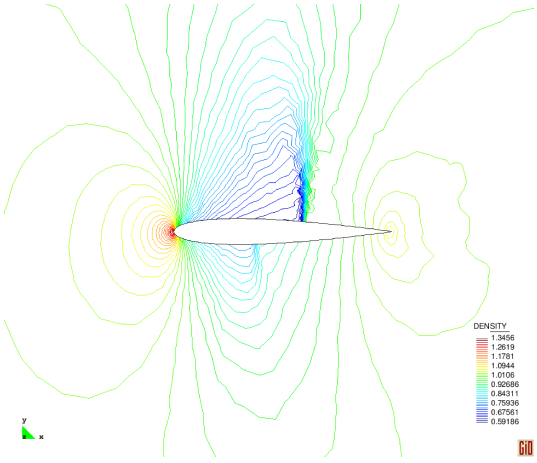

(a)

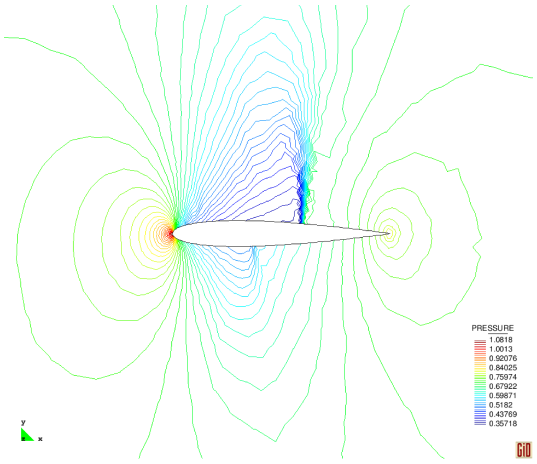

(b)

Figure 13: Transonic inviscid flow around a NACA0012 airfoil. Obtained solution for the initial mesh. (a) density contours and (b) pressure contours.

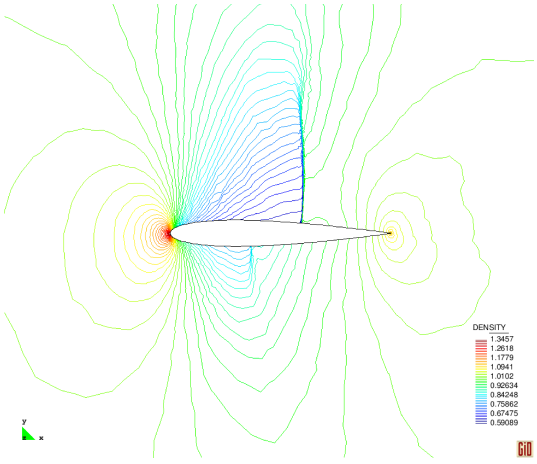

(a)

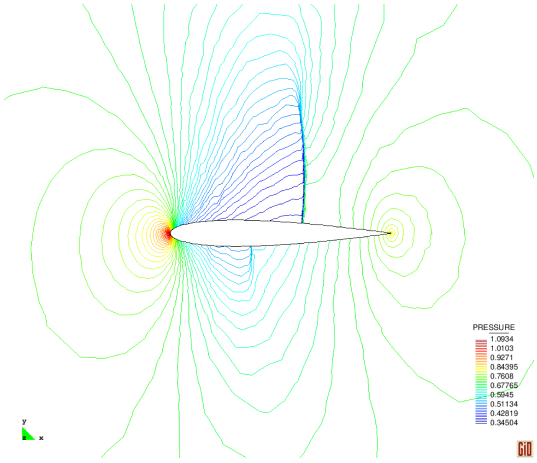

(b)

Figure 14: Transonic inviscid flow around a NACA0012 airfoil. Obtained solution for the adaptive mesh. (a) density contours and (b) pressure contours.

The pressure coefficient distribution over the airfoil resulting from the initial and adaptive meshes is graphically compared with the results of [70] in Figure 15 proving that accurate results have been obtained. Although the position of the shock does not change using the remeshing scheme, the adapted mesh improves the resolution in the high-gradient zones.

The pressure coefficient distribution over the airfoil resulting from the initial and adaptive meshes is graphically compared with the results of [70] in Figure 15 proving that accurate results have been obtained. It is observed that the shock position is slightly different from the reference results. The main reason is that the initial coarse mesh is not fine enough to capture the shock position, initially, in order to detect the regions where mesh refinement is needed. This difference can be improved by applying a finer initial mesh. Although the position of the shock does not change using the remeshing scheme, the adapted mesh improves the resolution in the high-gradient zones.

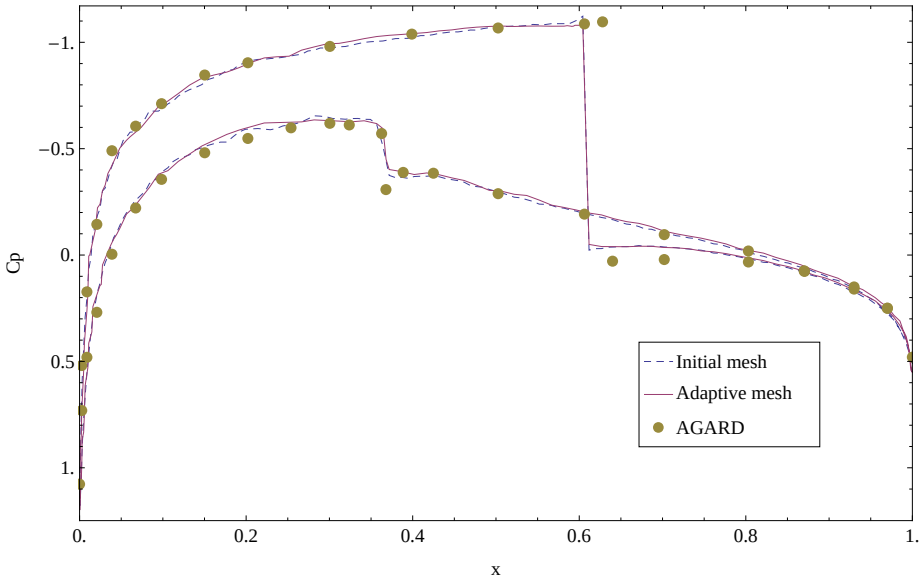

Figure 15: Transonic inviscid flow around a NACA0012 airfoil. Comparison of the c_p distributions with the reference values.

6.4 Example IV: Supersonic inviscid flow around a NACA0012 airfoil

The example involves the supersonic flow around a NACA0012 at $M_\infty = 1.2$ and $\alpha = 0.0°$ which is again evoked from the AGARD working group 07 [70]. The domain, the initial mesh and the boundary conditions are the same as for the Example III. Using a similar scheme for the mesh refinement, the final refined mesh is presented in Figure 16 containing 12245 nodes and 24759 elements.

The obtained solution using the initial and the adapted meshes are presented in Figures 17 and 18, respectively. It was found that although suitable results have been obtained using the initial mesh, the refinement scheme improves the quality of the results, especially near the shock waves. Also, both meshes are able to capture the shock waves near the leading and trailing edges of the airfoil.

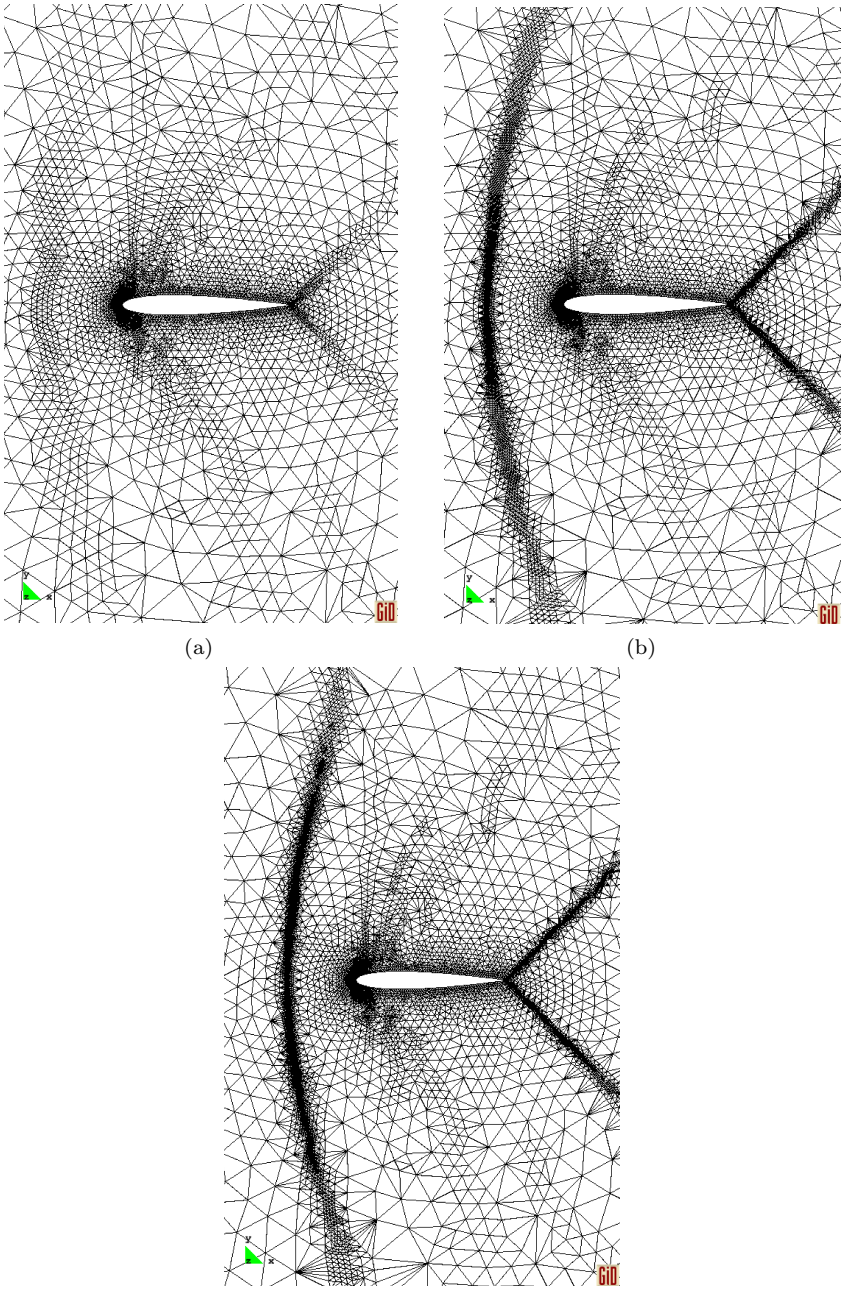

(a) (b)

(c)

Figure 16: Supersonic inviscid flow around a NACA0012 airfoil. Adaptive mesh after (a) one level, (b) three levels and (c) five levels of refinement.

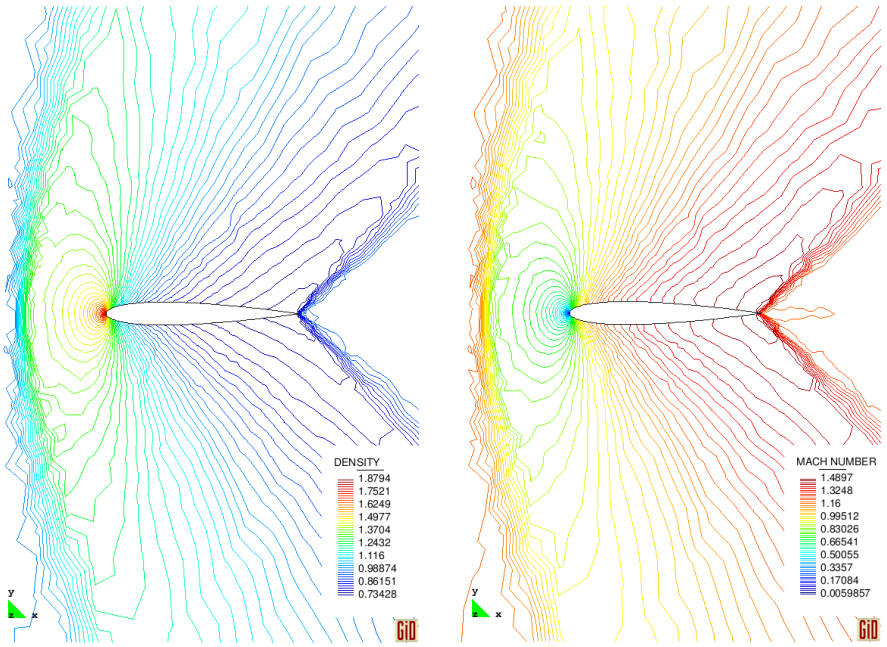

(a) (b)

Figure 17: Supersonic inviscid flow around a NACA0012 airfoil. Obtained solution for the initial mesh. (a) Density. (b) Mach number contours.

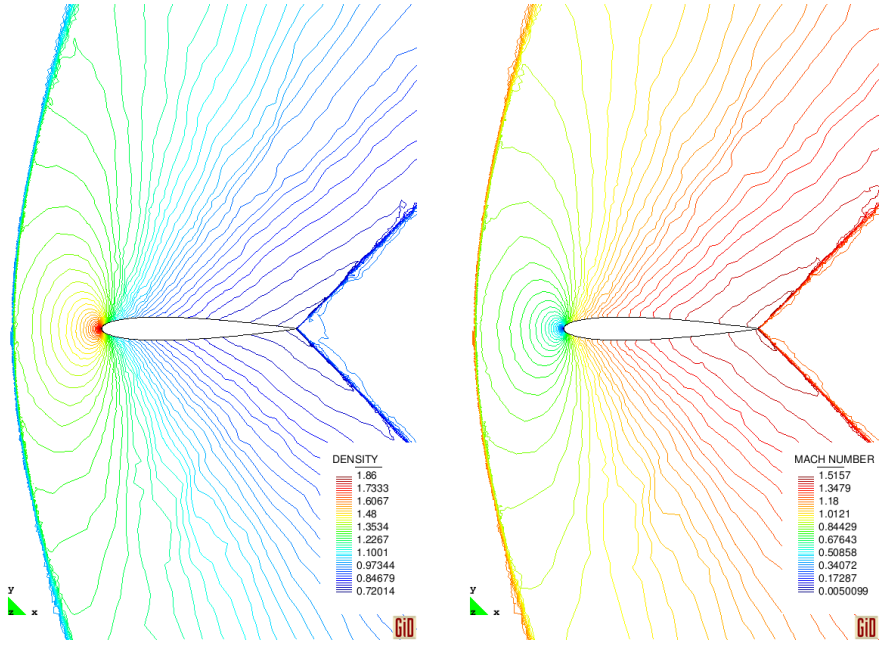

(a) (b)

Figure 18: Supersonic inviscid flow around a NACA0012 airfoil. Obtained solution for the refined mesh. (a) Density. (b) Mach number contours.

The pressure coefficient distributions over a NACA0012 surface obtained for this example are shown in Figure 19. Good agreement with the reference results can be observed using both meshes.

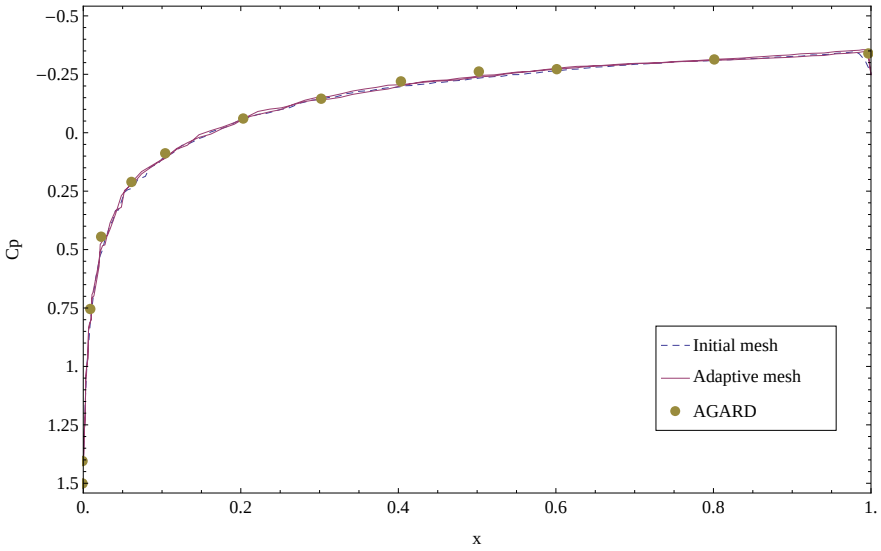

Figure 19: Supersonic inviscid flow around NACA0012 airfoil. The comparison of the c_p distributions with the reference values.

7 Concluding Remarks

Based on the concept of Finite Calculus (FIC), a new residual-based stabilized finite element method for solving the compressible Euler equations is presented. The method has been tested for 2D problems using 3-noded triangles, an unstructured meshes and an adaptive mesh refinement scheme. Different types of numerical examples have been studied to validate the features of the new methodology for subsonic, transonic and supersonic flows. The developed FIC-FEM stabilized formulation has led to stable and accurate solutions in regions where the flow has some complexities such as shock wave, stagnation point, etc. It was found that shocks are resolved within four or five elements. Appropriate pressure coefficient C_p distributions were also obtained along the boundary. Although the presented formulation has been able to provide suitable results using uniform meshes, error estimation and adaptive mesh refinement have improved the cost/accuracy ratio, especially for flows with shocks.

All these achievements can be considered as the basic tools for further developments of the proposed FIC method to more realistic applications like unsteady compressible flows and 3D problems. Viscous flows involving boundary layers and turbulence phenomena will be also considered as extensions of the present work.

8 Acknowledgements

The first author would like to acknowledge the financial support provided by CIMNE. We express our gratitude to Dr. Roberto Flores and Enrique Ortega for helpful discussions and suggestions.

This research was partially supported by the SAFECON project of the European Research Council.

References

[1] J. Von Neumann and R. D. Richtmyer. A method for the numerical calculation of hydrodynamic shocks. *J. Appl. Phys*, 21:232–237, 1950.

[2] R. Courant and E. Isaacson. On the solution of nonlinear hyperbolic differential equations by finite differences. *Comm. Pure and Applied Mathematics*, 5:243–255, 1952.

[3] P.D. Lax. Weak solutions of non-linear hyperbolic equations and their numerical approximations. *Communications on Pure and Applied Mathematics*, 7:159–193, 1954.

[4] S. K. Godunov. A difference scheme for numerical computation of discontinuous solution of hydrodynamic equations. *Matematicheskii Sbornik*, 47:271–306, 1959.

[5] B. Engquist and S. Osher. Stable and entropy satisfying approximations for transonic flow calculations. *Mathematics of Computation*, 34:45–75, 1980.

[6] P. L. Roe. The use of the Riemann problem in finite differenceschemes. *Lecture Notes in Physics*, 141:354–359, 1981.

[7] P. L. Roe. Approximate Riemann solvers, parameter vectors and difference schemes. *Journal Computational Physics*, 43:357–372, 1981.

[8] S. Osher. Shock modelling in aeronautics. *In, K. W. Morton and M. J. Baines(eds), NumericalMethodsfor Fluid Dynamics, London: AcademicPress*, pages 179–218, 1982.

[9] P. D. Lax and B. Wendroff. Difference schemes for hyperbolic equations with high order of accuracy. *Comm. Pure and Applied Mathematics*, 17:381–398, 1964.

[10] R.W. MacCormack. The effect of viscosity in hypervelocity impact cratering. *AIAA paper 69-0354, April-May*, 1969.

[11] A. Lerat and R. Peyret. Non centered schemes and shock propagation problems. *Computers and Fluids*, 2:35–52, 1969.

[12] A. Jameson, W. Schmidt, and E. Turkel. Numerical solution of the Euler equations by finite volume methods using Runge-Kutta time stepping schemes. *AIAA paper*, 81-1259, June 1981.

[13] W.K. Anderson, J.L. Thomas, and B. Van Leer. Comparison of finite volume flux vector splittings for the Euler equations. *AIAA Journal*, 24 (9):1453–1460, 1986.

[14] T.J.R. Hughes and T.E. Tezduyar. Finite element methods for first-order hyperbolic systems with particular emphasis on the compressible Euler equations. *Comput. Methods Appl. Mech. Engrg*, 45:217–284, 1984.

[15] T.J.R. Hughes, L.P. Franca, and M. Mallet. A new finite element formulation for computational fluid dynamics: VI. Convergence analysis of the generalized SUPG formulation for linear time-dependent multi-dimensional advective-diffusive systems. *Comput. Methods Appl. Mech. Engrg*, 63:97–112, 1987.

[16] A.N. Brooks and T.J.R. Hughes. Streamline upwind/Petrov-Galerkin formulations for convection dominated flows with particular emphasis on the incompressible Navier-Stokes equations. *Comput. Methods Appl. Mech. Engrg*, 32:199–259, 1982.

[17] S. Mittal and T. Tezduyar. A unified finite element formulation for compressible and incompressible flows using augmented conservation variables. *Comput. Methods Appl. Mech. Engrg*, 161:229–243, 1998.

[18] G.J. Le Beau and T.E. Tezduyar. Finite element computation of compressible flows with the SUPG formulation. *in: Advances in Finite Element Analysis in Fluid Dynamics, ASME, New York*, 123:21–27, 1991.

[19] J. Donea. A Taylor-Galerkin method for convective transport problems. *Int. J. Numer. Methods Engrg*, 20:101–120, 1984.

[20] F. Chalot and T.J.R. Hughes. A consistent equilibrium chemistry algorithm for hypersonic flows. *Comput. Methods Appl. Mech. Engrg*, 112:25–40, 1994.

[21] F. Shakib, T.J.R. Hughes, and Z. Johan. A new finite element formulation for computational fluid dynamics: X. The compressible Euler and Navier-Stokes equations. *Comput. Methods Appl. Mech. Engrg*, 89:141–219, 1991.

[22] G. Hauke and T.J.R. Hughes. A unified approach to compressible and incompressible flows. *Comput. Methods Appl. Mech. Engrg*, 113:389–395, 1994.

[23] A. J. Chorin. Numerical solution of the Navier-Stokes equations. *Math. Comput.*, 22:745–762, 1968.

[24] A. J. Chorin. Sur l'approximation de la solution des equations de Navier-Stokes par la methode des pas fractionaires (I). *Arch. Rat. Mech. Anal.*, 32:135–153, 1969.

[25] O.C. Zienkiewicz, R.L. Taylor, and P. Nithiarasu. *The Finite Element Method. Vol. 3 Fluid Dynamics.* Elsevier, 6th Edition, 2005.

[26] O.C. Zienkiewicz and R. Codina. A general algorithm for compressible and incompressible flow. Part I. The split characteristic based scheme. *Int. J. Numer. Methods Fluids.*, 20:869–885, 1995.

[27] O.C. Zienkiewicz, B.V.K. Satya Sai, K. Morgan, R. Codina, and M. Vazquez. A general algorithm for compressible and incompressible flow. Part II. Tests on the explicit form. *Int. J. Numer. Methods Fluids.*, 20:887–913, 1995.

[28] R. Codina, M. Vazquez, and O.C. Zienkiewicz. A general algorithm for compressible and incompressible flow. Part III: The semi-implicit form. *Int. J. Numer. Methods Fluids.*, 27:13–32, 1998.

[29] R. Codina. A discontinuity-capturing crosswind-dissipation for the finite element solution of the convection diffusion equation. *Comput. Methods Appl. Mech. Eng*, 110:325–342, 1993.

[30] J. Peraire, J. Peiro, L. Formaggia, K. Morgan, and O.C. Zienkiewicz. Finite element Euler computations in three dimensions. *Int. J. Numer. Methods Eng.*, 26:2135–2159, 1988.

[31] K. Morgan, J. Peraire, J. Peiro, and O.C. Zienkiewicz. Adaptive remeshing applied to the solution of a shock interaction problem on a cylindrical leading edge. *in P. Stow (ed.), Computational Methods in Aeronautical Fluid Dynamics, Clarenden Press, Oxford*, pages 327–344, 1990.

[32] O.C. Zienkiewicz and J. Wu. A general explicit of semi-explicit algorithm for compressible and incompressible flows. *Int. J. Numer. Methods Eng.*, 35:457–479, 1992.

[33] T.J.R. Hughes. Greens functions, the Dirichlet-to-Neumann formulation, subgrid scale models, bubbles and the origins of stabilized method. *Comp. Meth. Appl. Mech. Eng*, 127:387–401, 2007.

[34] G. Scovazzi. A discourse on Galilean invariance, SUPG stabilization, and the variational multiscale framework. *Comp. Meth. Appl. Mech. Eng*, 196(4-6):1108–1132, 2007.

[35] G. Scovazzi. Galilean invariance and stabilized methods for compressible flows. *Int. J. Num. Meth. Fluids*, 54(6-8):757–778, 2007.

[36] J. Donea and A. Huerta. *Finite Element Methods for Flow Problems.* Wiley, 2003.

[37] G. Scovazzi, M.A. Christon, T.J.R. Hughes, and J.N. Shadid. Stabilized shock hydrodynamics: I. A Lagrangian method. *Comp. Meth. Appl. Mech. Eng*, 196(4-6):923–966, 2007.

[38] G. Scovazzi, J.N. Shadid, E. Love, and W.J. Rider. A conservative nodal variational multiscale method for Lagrangian shock hydrodynamics. *Comp. Meth. Appl. Mech. Eng*, 199(49-52):3059–3100, 2010.

[39] G. Scovazzi. Lagrangian shock hydrodynamics on tetrahedral meshes. A stable and accurate variational multiscale approach. *J. Comput. Phys.*, 231:8029–8069, 2012.

[40] B. Van Leer. Towards the ultimate conservative difference scheme. II. Monotonicity and conservation combined in a second-order scheme. *J. Comput. Phys.*, 14(4):361–370, 1974.

[41] B. Van Leer. Towards the ultimate conservative difference scheme III. Upstream-centered finite-difference schemes for ideal compressible flow. *J. Comput. Phys.*, 23 (3):263–275, 1977.

[42] R. J. LeVeque. *Numerical methods for conservation laws (Second ed.)*. Birkhauser, 1992.

[43] J. P. Boris and D. L. Book. Flux corrected transport I. SHASTA, a fluid transport algorithm that works. *J. Comput. Phys.*, 11:38–69, 1973.

[44] A. Harten. High resolution schemes for hyperbolic conservation laws. *J. Comput. Phys.*, 49:357–393, 1983.

[45] S.T. Zalesak. Fully multidimensional Flux-Corrected Transport algorithm for fluids. *J. Comput. Phys.*, 31:335–362, 1979.

[46] A. K. Parrott and M. K. Christie. FCT applied to the 2D finite element solution of tracer transport by single phase flow in a porous medium. *Numerical Methods for Fluid Dynamics, Oxford: Oxford University Press*, pages 27–53, 1986.

[47] R. Löhner, K. Morgan, J. Peraire, and M. Vahdati. Finite element flux-corrected transport (FEM-FCT) for the Euler and Navier-Stokes equations. *Int. J. Num. Methods Fluids*, 7:103–109, 1987.

[48] H. Luo, J. D. Baum, R. Löhner, and J. Cabello. Adaptive edge-based finite element schemes for the Euler and Navier-Stokes equations. *AIAA-93-0336*, 1993.

[49] R. Sanders. On convergence of monotone finite difference schemes with variable spatial differencing. *Math. Comp.*, 40:91–106, 1983.

[50] A. Jameson and P.D. Lax. Conditions for the construction of multi-point Total Variation Diminishing difference schemes. *MAE Report 1650, Dept . of Mechanical and Aerospace Engineering, Princeton University*, 1984.

[51] S.F. Davis. TVD finite difference schemes and artificial viscosity. *ICASE Report No. 84-20*, 1984.

[52] H.C. Yee. Construction of implicit and explicit symmetric TVD schemes and their applications. *J. Comput. Phys.*, 68:151–179, 1987.

[53] H.C. Yee and P. Kutler. Application of second-order accurate Total Variation Diminishing (TVD) schemes to the Euler equations in general geometries. *NASA TM-85845*, 1983.

[54] M. Aftosmis and N. Kroll. A quadrilateral based second-order TVD method for unstructured adaptive meshes. *AIAA-91-0124*, 1991.

[55] P. R. M. Lyra, K. Morgan, J. Peraire, and J. Peiro. TVD algorithms for the solution of the compressible Euler equations on unstructured meshes. *Int. J. Numer. Methods Flu.*, 19(9):827–847, 1994.

[56] D. Kuzmin and S. Turek. High-resolution FEM-TVD schemes based on a fully multidimensional flux limiter. *J. Comput. Phys.*, 198:131–158, 2004.

[57] E. Oñate. Derivation of stabilized equations for advective-diffusive transport and fluid flow problems. *Comput. Meth. Appl. Mech. Engng.*, 151:233–267, 1998.

[58] E. Oñate, J. Garcia, and S. Idelsohn. An alpha-adaptive approach for stabilized finite element solution of advective-diffusive problems with sharp gradients. *New Adv. in Adaptive Comp. Met. in Mech., P. Ladeveze and J.T. Oden (Eds.), Elsevier*, 1998.

[59] E. Oñate and M. Manzan. A general procedure for deriving stabilized space-time finite element methods for advective-diffusive problems. *Int. J. Num. Meth. Fluids.*, 31:203–221, 1999.

[60] E. Oñate. A stabilized finite element method for incompressible viscous flows using a finite increment calculus formulation. *Comp. Meth. Appl. Mech. Eng*, 182:355–370, 2000.

[61] E. Oñate and J. Garcia. A finite element method for fluid-structure interaction with surface waves using a finite calculus formulation. *Comput. Meth. Appl. Mech. Eng.*, 191:635–660, 2001.

[62] E. Oñate. Possibilities of finite calculus in computational mechanics. *Int. J. Num. Meth. Engng*, 60:255–281, 2004.

[63] R. Löhner. Mesh adaptation in fluid mechanics. *Engineering Fracture Mechanics*, 50(5/6):819–847, 1995.

[64] C. Hirsch. *Numerical Computation of Internal and External Flow, Vol. 1.* J. Wiley, New York, 1988 (vol. 2, 1990).

[65] D.J. Mavriplis, A. Jameson, and L. Martinelli. Multigrid solution of the Navier-Stokes equations on triangular meshes. *ICASE Rep. No. 89-11*, 1989.

[66] E. Turkel. Improving the accuracy of central difference schemes. *ICASE Report 8853*, 1988.

[67] R. Löhner. An adaptive finite element solver for transient problems with moving bodies. *Comput. and Structures*, 30:303–317, 1988.

[68] R. Löhner. Three-dimensional grid generation by the advancing front method. *International Journal for Numerical Methods in Fluids*, 8:1135–1149, 1988.

[69] R. Löhner and J. D. Baum. Adaptive H-refinement on 3-D unstructured grids for transient problems. *International Journal for Numerical Methods in Fluids*, 14(12):1407–1419, 1992.

[70] T. H. Pulliam and J. T. Barton. Euler computations of AGARD working group 07 airfoil test cases. *AIAA Paper 85-0018, AIAA 23rd Aerospace Sciences Meeting*, Nev. 1985.